Effects of density-dependent weak form factors on neutral-current neutrino (antineutrino)-neucleus scattering in the quasi-elastic region

K. S. Kim,[1] Myung-Ki Cheoun,[2] W. Y. So,[3] and Hungchong Kim[4]
[1]*School of Liberal Arts and Science, Korea Aerospace University, Goyang 412-791, Korea*
[2]*Department of Physics, Soongsil University, Seoul 156-743, Korea*
[3]*Department of Radiological Science, Kangwon National University, Samcheok 245-711, Korea*
[4]*Department of General Education, Kookmin University, Seoul 136-702, Korea*
(Received 21 August 2014; published 13 January 2015)

We study the effects of density-dependent weak vector form factors on the inclusive neutral-current–neutrino (antineutrino)-nucleus scattering in the quasi-elastic region within the framework of a relativistic single-particle model. The density-dependent weak form factors are obtained from a quark-meson coupling model. The density-dependence effects are studied separately in protons and neutrons participating in the reactions, in each response cross section, and with regard to asymmetry. These density effects reduce the cross section at high densities and show different behavior with regard to asymmetry. Furthermore we calculate flux-averaged differential cross sections and compare them with the experimental data.

DOI: 10.1103/PhysRevC.91.014606 PACS number(s): 25.30.Pt, 13.15.+g, 13.40.Gp, 24.10.Jv

I. INTRODUCTION

Neutrino interactions provide valuable information on various domains of physics such as astrophysics, particle physics, and nuclear physics. In particular, the neutrino-nucleus (ν-A) scattering is one of the useful tools in studying weak interaction, properties of the nucleus, and so on. Neutral-current (NC) ν-A scattering is more effective to investigate the nuclear structure because of there is no Coulomb distortion of outgoing leptons from the target nucleus. Moreover, NC scattering could be the alternative to parity-violating electron scattering [1,2], which measures matter distribution of finite nuclei, because of the intermediate Z^0 boson in the NC scattering [3–5].

Since the first measurement of NC muon neutrino (ν_μ) scattering at Brookhaven National Laboratory [6], the MiniBooNE Collaboration has recently performed the charged-current reaction (CC) [7] and the NC [8] from a CH_2 target. In particular, the MiniBooNE data, which measured the flux-averaged NC elastic cross sections in the quasi-elastic region, can be explained by nonstandard values of the axial mass and the strange axial form factor at $Q^2 = 0$, $M_A = 1.39$ GeV, and $g_A^s = 0.08$. Other MiniBooNE data obtained from antineutrino scattering experiments [9,10] can be explained using the fit with $M_A = 1.39$ GeV in the analysis, but the fit with $M_A = 1.02$ GeV is also shown to be compatible with the data.

Since the publication of the MiniBooNE data [7,8] for $^{12}C(\nu_\mu,\mu^-)$ and $^{12}C(\nu,\nu')$ scattering, there have been many theoretical works [11–16]. Nieves *et al.* [11] calculated the CC double cross section by including random-phase approximation (RPA) correlations and multinucleon contributions based on the Fermi gas model and then deduced the increase of the value of the axial mass. Meucci *et al.* [12] calculated the CC quasi-elastic cross section in the framework of a relativistic mean-field (RMF) model utilizing the relativistic Green function method. They found that the relativistic Green function results may describe the experimental data for total cross sections without additional adjustment of the nucleon axial mass. Butkevich and Perevalov [13] calculated the NC reaction with the relativistic distorted-wave impulse approximation (RDWIA) and extracted the axial strange form factor $g_A^s = -0.11$ by using the MiniBooNE data from $(\nu p \to \nu p)/(\nu N \to \nu N)$ in the high-energy region. Ankowski [14] calculated the $^{12}C(\nu_\mu,\mu^-)$ scattering, the results of which underestimated the MiniBooNE data by 20% with the axial mass 1.23 GeV, but overestimated the data by 15% with the axial mass 1.39 GeV. Amaro *et al.* [15] tried to explain the muon neutrino cross section [7] by using the superscaling approach (SuSA) with inclusion of the meson-exchange current in the two-particle–two-hole (2p-2h) sector. Their results do not seem to describe the data well at large scattering angle and low muon energy. Gonzalez-Jimenez *et al.* [16] calculated the NC neutrino scattering based on the RMF and SuSA models and estimated the ratio $(\nu p \to \nu p)/(\nu N \to \nu N)$.

On the other hand, since the first discovery of the "EMC" effect [17], the possible medium modifications of nucleon form factors have been studied over 30 years. Among various approaches, two theoretical models, which have exploited the modifications of the electric and magnetic form factors of nucleons in the nuclear medium, might be interesting. These are the quark-meson coupling (QMC) model proposed by Thomas and collaborators [18] and the cloudy bag model by Cheon and Jeong [19]. In specific, by using the QMC model, Thomas and collaborators [20] calculated the density dependence of weak form factors. This model successfully described various properties of hadrons in nuclear matter [21], finite nuclei [22], and hypernuclei [23]. The authors of Ref. [22] found a simple scaling relation for the change of the hadron masses, which was described in terms of the number of nonstrange quarks in a hadron and the strength of the scalar mean field in a nucleus. In Ref. [24], the $^{12}C(\nu_\mu,\mu^-)X$ reaction was calculated using the density-dependent weak form factors within a relativistic Fermi gas model and then the bound nucleon form factors were found to reduce total cross sections by 8% (or higher for a heavier nucleus).

The ratio of G_E/G_M for protons was measured at the Thomas Jefferson National Accelerator Facility (JLab) [25] in $\vec{e}p \to e\vec{p}$ scattering in terms of high Q^2. Another experiment at JLab was performed to measure the transverse and longitudinal responses of the polarized knocked-out proton in the reaction ^{16}O$(\vec{e},e'\vec{p})$ in quasi-elastic perpendicular kinematics at $Q^2 = 0.8\,(\mathrm{GeV}/c)^2$ in terms of the missing momentum [26]. The ratio of the transverse to longitudinal polarization transfer for the proton from ^{16}O agreed with theoretical calculations from free proton form factors.

In our previous articles [27,28], we studied the effects of density-dependent weak form factors on the CC and NC reactions of the ν-A scattering within the framework of the quasi-particle random-phase approximation (QRPA) in the low-energy range ($E_{\nu(\bar{\nu})} \leqslant 80$ MeV). Neutrino reaction cross sections at normal nuclear density, ρ_0, can be reduced by 5% at most, but, in $\bar{\nu}$-A reactions, the cross sections are substantially decreased in the nuclear medium, up to 35% in comparison with the calculations using the free form factors. Also, in the quasi-elastic region, the effect of the density-dependent weak form factor on the CC neutrino-nucleus scattering from ^{12}C, ^{40}Ca, and ^{208}Pb was estimated, and the cross section was reduced maximally by 60% at $\rho = 2.0\rho_0$ for the antineutrino around the peak position [29].

In this work, we extend our previous calculations [27–29] and investigate the in-medium effects by the density-dependent weak form factors for the inclusive NC $\nu(\bar{\nu})$-A scattering from ^{12}C. Specifically, we focus on the roles of each density-dependent form factor in the weak current. For this calculation, a relativistic single-particle model requires bound-state and continuum-nucleon wave functions and a transition current operator. The bound nucleon wave functions are generated by solving the Dirac equation in the presence of the strong scalar and vector potentials of the σ-ω model self-consistently [30]. The wave functions of the knocked-out nucleons are also generated by the same potential of the bound nucleons, called the RMF. This RMF model guarantees the current conservation and gauge invariance and provides very good agreement with the Bates (e,e') experimental data with the inclusion of the Coulomb distortion of the electrons [31]. Our results are compared with flux-averaged differential-cross-section data measured by the MiniBooNE Collaboration [8].

In Sec. II we briefly introduce the formalism for the ν-A scattering. Our theoretical results are presented in Sec. III with the cross sections and asymmetry. Finally, the summary and conclusion are given in Sec. IV.

II. FORMALISM

We choose the nucleus fixed frame where the target nucleus is seated at the origin of the coordinate system. The four-momenta of incident and outgoing $\nu(\bar{\nu})$ are labeled $p_i^\mu = (E_i, \mathbf{p}_i)$ and $p_f^\mu = (E_f, \mathbf{p}_f)$, respectively. p_A^μ, p_{A-1}^μ, and p^μ represent the four-momenta of the target nucleus, the residual nucleus, and the final nucleon, respectively. In the laboratory frame, the differential cross section is given by the contraction between the lepton and the hadron tensors [32]:

$$\frac{d\sigma}{dT_N} = 4\pi^2 \frac{M_N M_{A-1}}{(2\pi)^3 M_A} \int \sin\theta_l d\theta_l \int \sin\theta_N d\theta_N\, p f_{\mathrm{rec}}^{-1} \sigma_M^Z \times [v_L R_L + v_T R_T + h v_T' R_T'], \quad (1)$$

where M_N is the nucleon mass, θ_l denotes the scattering angle of the lepton, and $h = -1$ ($h = +1$) corresponds to the helicity of the incident $\nu(\bar{\nu})$. θ_N and T_N represent the polar angle and the kinetic energy of the knocked-out nucleons, respectively. Detailed forms for the kinematical coefficients v and the corresponding response functions R for ν-A scattering are given in Refs. [32,33]. In Eq. (1), the first term refers to the longitudinal term, the second the transverse term, and the last the interference term.

For the NC reaction, σ_M^Z is defined as

$$\sigma_M^Z = \left(\frac{G_F \cos(\theta_l/2) E_f M_Z^2}{\sqrt{2}\pi \left(Q^2 + M_Z^2\right)} \right), \quad (2)$$

where M_Z is the rest mass of the Z boson and G_F is the Fermi constant. The recoil factor f_{rec} is given by

$$f_{\mathrm{rec}} = \frac{E_{A-1}}{M_A} \left| 1 + \frac{E_p}{E_{A-1}} \left[1 - \frac{\mathbf{q}\cdot\mathbf{p}}{p^2} \right] \right|. \quad (3)$$

In a plane-wave Born approximation, where leptons are described as Dirac plane waves, the cross sections for the inclusive ν-A scattering are calculated straightforwardly (e.g., see Refs. [32,33]). The weak current J^μ represents the Fourier transform of the nucleon current density written as

$$J^\mu = \int \bar{\psi}_p \hat{\mathbf{J}}^\mu \psi_b e^{i\mathbf{q}\cdot\mathbf{r}} d^3r, \quad (4)$$

where $\hat{\mathbf{J}}^\mu$ is a free weak nucleon current operator, and ψ_p and ψ_b are wave functions of the knocked-out and the bound-state

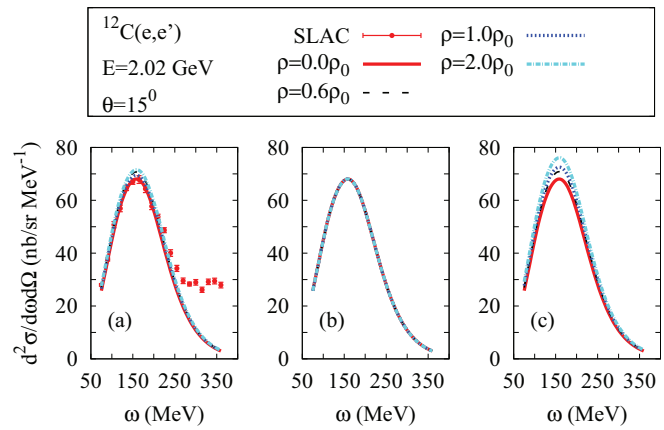

FIG. 1. (Color online) The differential cross sections of the inclusive (e,e') reaction in terms of the energy transfer for the incident electron energy 2.02 GeV from ^{12}C. Solid (red) curves are the results for no density-dependence, dashed (black) curves are for $\rho = 0.6\rho_0$, dotted (blue) curves are for $\rho = 1.0\rho_0$, and dash-dotted (sky blue) curves are for $\rho = 2.0\rho_0$. The experimental data come from the Stanford Linear Accelerator Center (SLAC) [35]. The explanations of the panels (a), (b), and (c) are in the context. Results for $\rho = 0.6\rho_0$ are shown for the presumed Fermi momentum of ^{12}C.

nucleon, respectively. For a free nucleon of the NC reaction, the current operator comprises the weak vector and the axial vector form factors:

$$\hat{\mathbf{J}}^{\mu} = F_1^V(Q^2)\gamma^{\mu} + F_2^V(Q^2)\frac{i}{2M_N}\sigma^{\mu\nu}q_{\nu} + G_A(Q^2)\gamma^{\mu}\gamma^5. \tag{5}$$

The vector form factors for the proton (neutron), $F_i^{V,p(n)}(Q^2)$, are expressed as

$$F_i^{V,p(n)}(Q^2) = \left(\tfrac{1}{2} - 2\sin^2\theta_W\right) F_i^{p(n)}(Q^2) - \tfrac{1}{2}F_i^{n(p)}(Q^2) - \tfrac{1}{2}F_i^s(Q^2), \tag{6}$$

where θ_W is the Weinberg angle given by $\sin^2\theta_W = 0.2224$.

The strange vector form factor $F_i^s(Q^2)$ in Eq. (6) is usually given as a dipole form, independently of the nucleon isospin:

$$F_1^s(Q^2) = \frac{F_1^s(0)Q^2}{(1+\tau)\left(1+Q^2/M_V^2\right)^2}, \qquad F_2^s(Q^2) = \frac{F_2^s(0)}{(1+\tau)\left(1+Q^2/M_V^2\right)^2}, \tag{7}$$

where $\tau = Q^2/(4M_N^2)$ and $M_V = 0.843$ GeV is the cutoff mass parameter usually adopted for nucleon electromagnetic form factors. $F_1^s(0)$ is defined as the squared strange radius of the nucleus, $F_1^s(0) = dG_E^s(Q^2)/dQ^2|_{Q^2=0} = 0.53\ \text{GeV}^{-2}$, and $F_2^s(0) = \mu_s = -0.4$ is an anomalous strange magnetic moment.

The axial form factors are given by

$$G_A(Q^2) = \tfrac{1}{2}\left(\mp g_A + g_A^s\right)\Big/\left(1+Q^2/M_A^2\right)^2, \tag{8}$$

where $g_A = 1.262$, $M_A = 1.032$ GeV, and $g_A^s = -0.19$, which represents the strange quark contents on the nucleon [34]. $-(+)$ coming from the isospin dependence denotes the knocked-out proton (neutron), respectively. The g_A^s represents the strange quark contents in the nucleon.

In this work, we introduce just the density dependence of the weak form factors multiplying the free form factors in previous expressions by $R(F_{1,2}^V) = F_{1,2}^V(\rho, Q^2)/F_{1,2}^V(\rho = 0, Q^2)$, which is generated by the QMC model [20]. In this way, the free result for all cross sections and contributions is recovered for the $\rho = 0$ case. Detailed features of the form factors and their modifications in nuclear matter used in this study are found in Refs. [27,28]. Of course, the weak form factors including the axial form factor are shown to be recovered from the

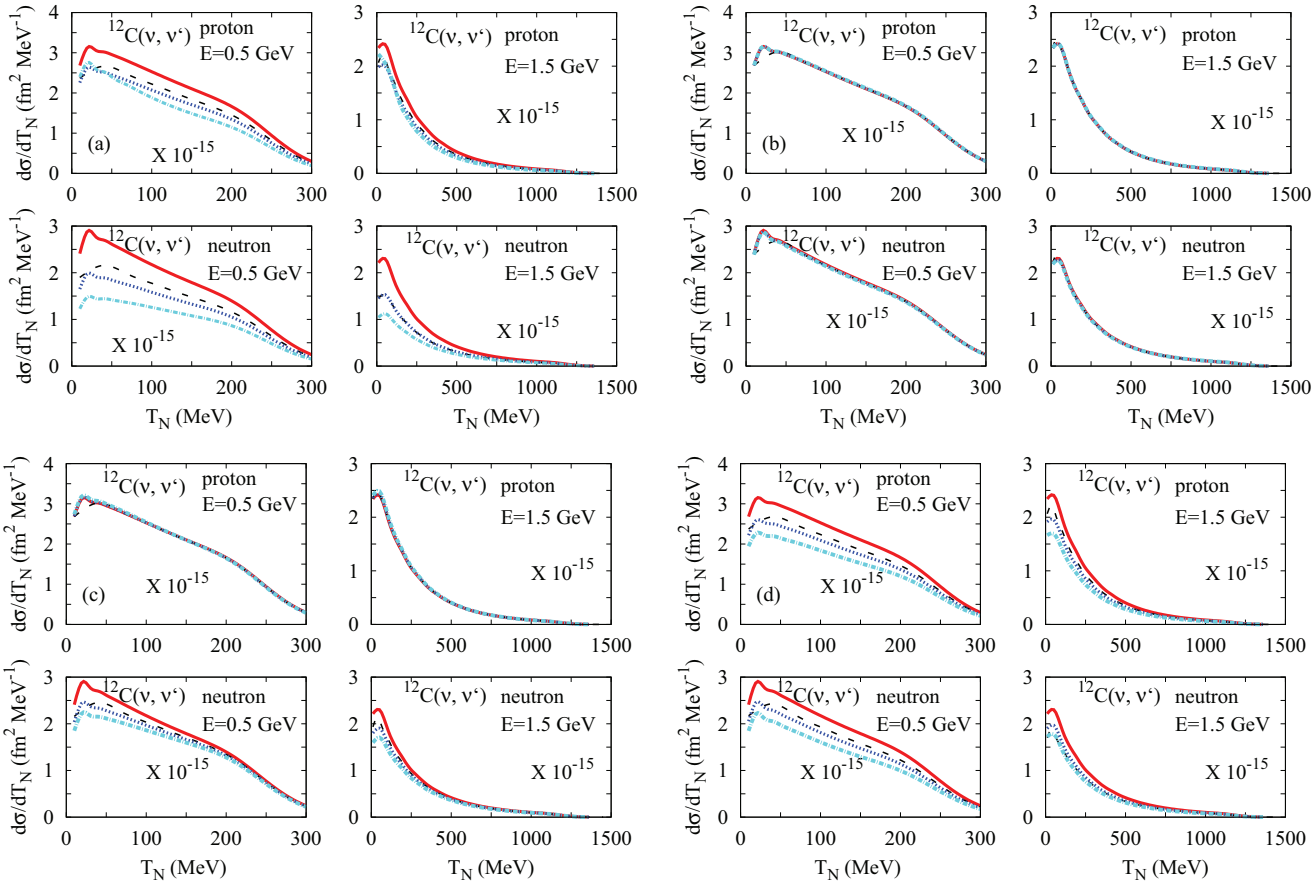

FIG. 2. (Color online) The differential cross sections of the inclusive (ν,ν') scattering in terms of the kinetic energy of the knocked-out nucleon for the incident ν energies 0.5 and 1.5 GeV from ^{12}C. Solid (red) curves are the results for no density-dependence, dashed (black) curves are for $\rho = 0.6\rho_0$, dotted (blue) curves are for $\rho = 1.0\rho_0$, and dash-dotted (sky blue) curves are for $\rho = 2.0\rho_0$. The explanations of the panels (a), (b), (c), and (d) are in the context.

standard form factors at the $\rho = \rho_0$ limit in the Appendix of Ref. [28].

III. RESULTS

To investigate the effects of density dependence we calculate the inclusive (e,e') reaction as shown in Fig. 1. The incident electron energy is 2.02 GeV and the scattering angle is 15°. The experimental data were measured at the Stanford Linear Accelerator Center [35]. Solid (red) curves are the results for no density-dependence, dashed (black) curves are for $\rho = 0.6\rho_0$, dotted (blue) curves are for $\rho = 1.0\rho_0$, and dash-dotted (sky blue) curves are for $\rho = 2.0\rho_0$. Figure 1(a) shows the results including the density dependence of all form factors (F_1 and F_2), Fig. 1(b) shows the results including only the density dependence of the Dirac form factor F_1, and Fig. 1(c) shows the results allowing the density dependence on the Pauli form factors F_2. The effects of the density dependence on F_1 reduce the cross section in Fig. 1(b) less than 1% but those on F_2 enhance the cross section. However, the in-medium effects in the electron scattering turn out to be not as large as that of neutrino scattering as shown later on. The reason comes from the absence of the axial current in the electron scattering. Namely, the in-medium effect on the axial form factor is larger than the electromagnetic form factors. In this work, the choice of $\rho = 0.6\rho_0$ is due to the density of ^{12}C. Note that $\rho_0 \sim 0.15$ fm^{-3} is the normal density.

Next we present our numerical results for the NC scattering with detailed discussions regarding the density-dependent effects. As shown in Fig. 2, we calculate the inclusive (ν,ν') reaction in terms of the kinetic energy of the knocked-out nucleon. Solid (red) curves are the results for no density-dependence, dashed (black) curves are for $\rho = 0.6\rho_0$, dotted (blue) curves are for $\rho = 1.0\rho_0$, and dotted (sky blue) curves are for $\rho = 2.0\rho_0$. Figure 2(a) (four panels in the upper left) shows the results including the density dependence of all form factors (F_1, F_2, and G_A) and Fig. 2(b) (four panels in the upper right) shows the results including only the density dependence of the Dirac form factor F_1, where the density dependence on F_2 and G_A is not taken into account. Similarly, Figs. 2(c) (four panels in the lower left) and 2(d) (four panels in the lower right) show the results allowing the density dependence on the Pauli form factor F_2 and the axial form factor G_A, respectively.

In general, the effects from the density dependence of each form factor in neutrino scattering are larger on neutrons than on protons. Also these effects decrease as the incident ν energy increases. In particular, the effects on F_1 [Fig. 2(b)] are very small in both protons and neutrons. Furthermore, the effect is largest on G_A [Fig. 2(d)] because the vector terms is canceled out each other in Eq. (6). The decreasing pattern of

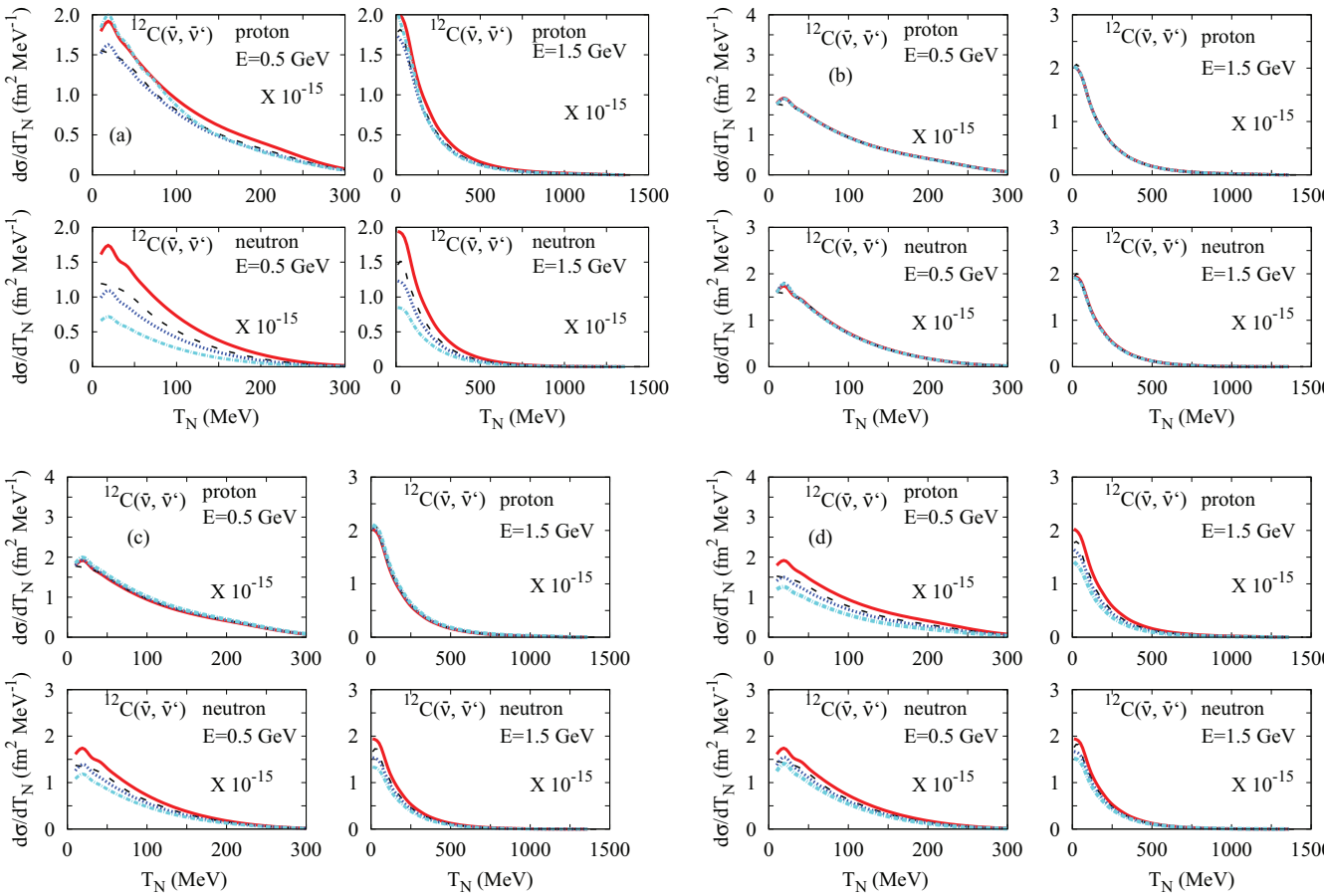

FIG. 3. (Color online) The same as Fig. 2, but for antineutrino.

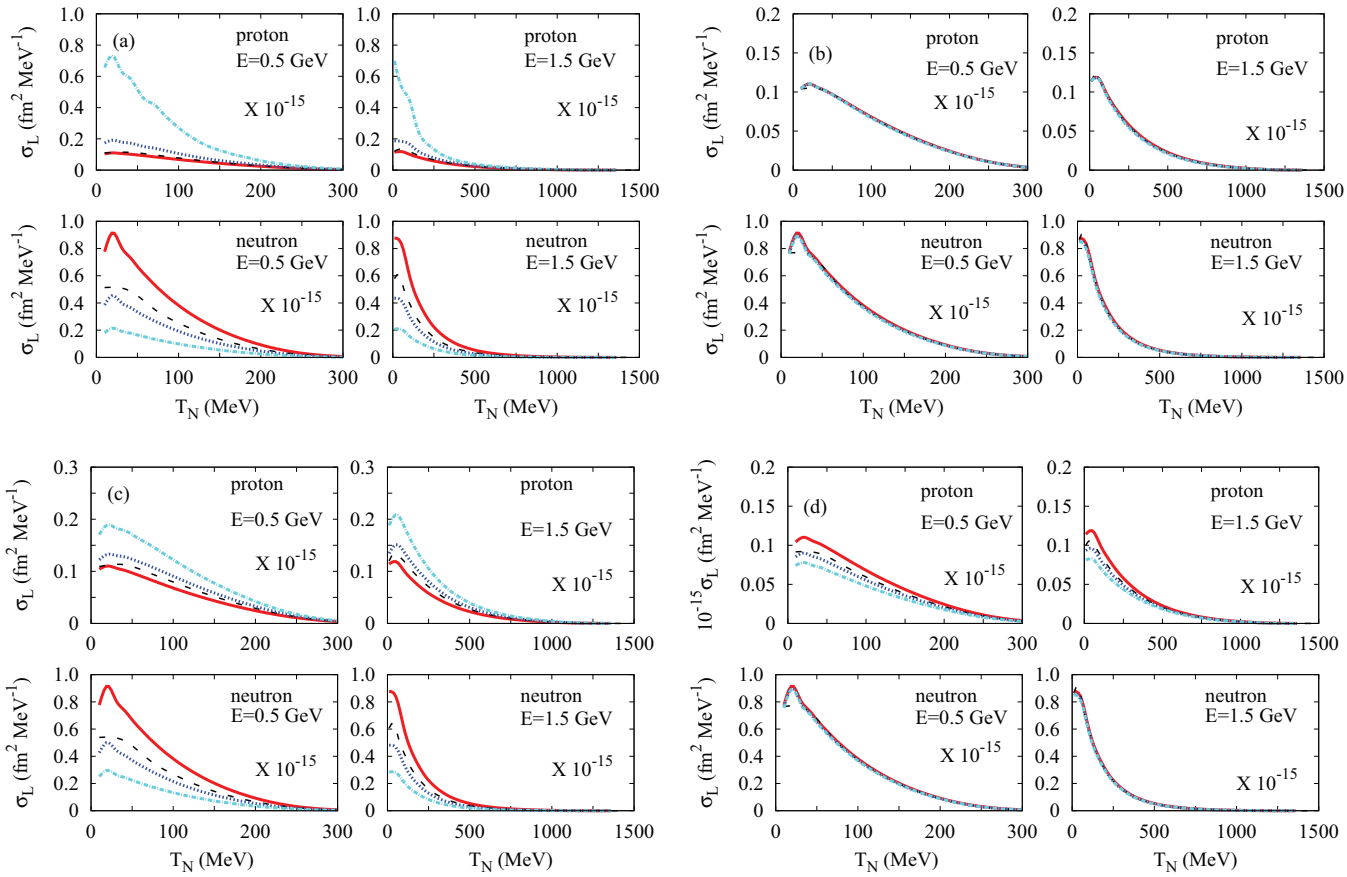

FIG. 4. (Color online) The longitudinal cross sections for inclusive (ν,ν') scattering with the same kinematics as in Fig. 2.

NC scattering is similar to that of CC scattering investigated in our previous calculation [29].

In Fig. 3, we present the differential cross sections for the $\bar{\nu}$-A scattering versus the kinetic energy of a knocked-out nucleon. The kinematics and the explanation of the curves are the same as the previous ones in Fig. 2. The density effects on $\bar{\nu}$-A scattering are a little bit smaller than those on (ν-A) scattering. The shapes of the cross sections are similar to the corresponding cross sections of ν-A scattering but the magnitudes are reduced by up to 25% in the case of neutrons. Therefore cross sections of $\nu(\bar{\nu})$-A scattering are generally reduced about 20%∼30% by the density dependence, irrespective of scattering modes of NC and CC and neutrino helicity.

Next we calculate and present the longitudinal, transverse, and interference part of the cross sections as given in Eq. (1). The nuclear response functions cannot be separated due to the integration of the scattering angle. Because the difference between the incident ν and $\bar{\nu}$ is only the intrinsic helicity as shown in Eq. (1), first we calculate the longitudinal and the transverse cross sections for the case of the incident ν. Figure 4 shows the longitudinal cross sections for inclusive (ν,ν') scattering with the same kinematics as the previous calculations in Fig. 2. The density dependence increases the longitudinal cross sections for the proton case and decreases the ones for the neutron. Similarly as in the previous results, the effects due to F_1 are very small. The effects on the neutron are larger for F_2 than those on the proton, and for G_A on the neutron are smaller than those on the proton. The effects are largest for F_2 and are almost independent of the incident energy.

As shown in Fig. 5, we present the transverse cross sections, which are the second term in Eq. (1). The effects are nearly negligible on F_1 and F_2 but on G_A they reduce the transverse cross sections about 30%. Hence the main contribution of the density dependence is to G_A. Because the transverse cross sections are about 10 times larger than the longitudinal cross sections, most medium effects are thought to occur in the transverse cross section.

Figure 6 shows the interference cross sections, which are the third term in Eq. (1). The effects on F_1 and F_2 are small but on G_A they reduce the interference cross sections. Hence the main contribution of the density dependence is to G_A, similar to the contribution of the transverse cross sections. In particular, the shape of the interference term is different from that of other terms. From Figs. 4–6, it can be seen that the transverse cross sections' biggest contribution is to the magnitude and the main effects of the density-dependent form factors show up on the transverse cross sections.

As an alternative way to investigate the effects of the density dependence, we introduce an asymmetry on the ν and $\bar{\nu}$ cross

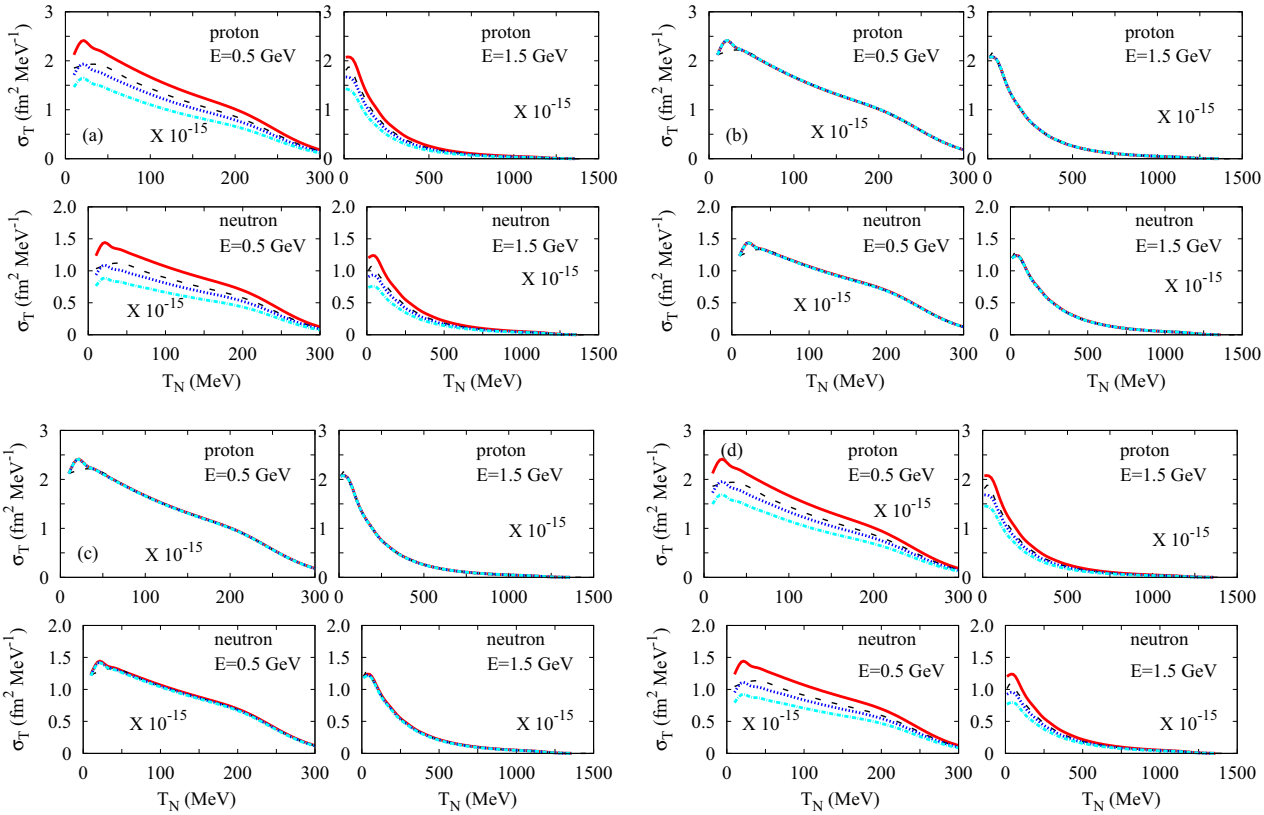

FIG. 5. (Color online) The transverse cross sections for inclusive (ν,ν') scattering with the same kinematics as in Fig. 2.

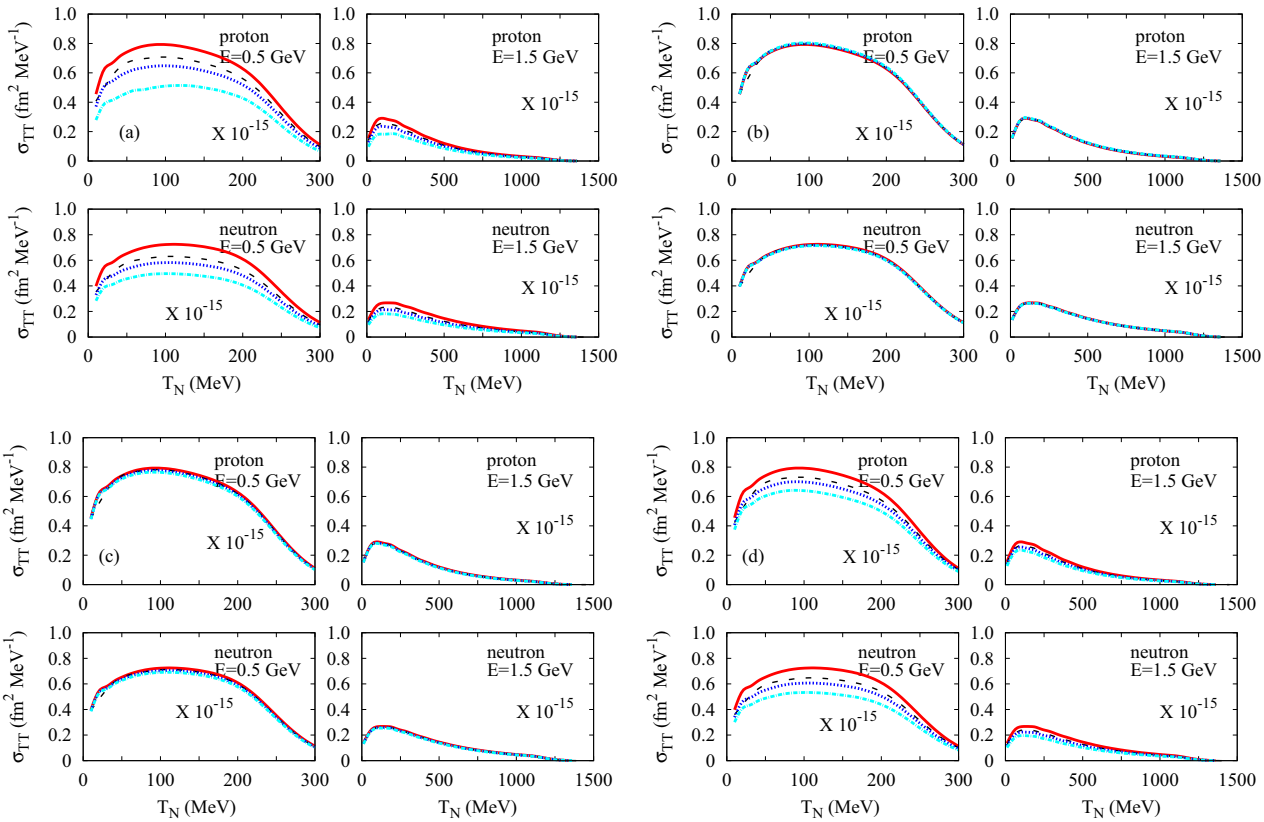

FIG. 6. (Color online) The interference cross sections for inclusive (ν,ν') scattering with the same kinematics as in Fig. 2.

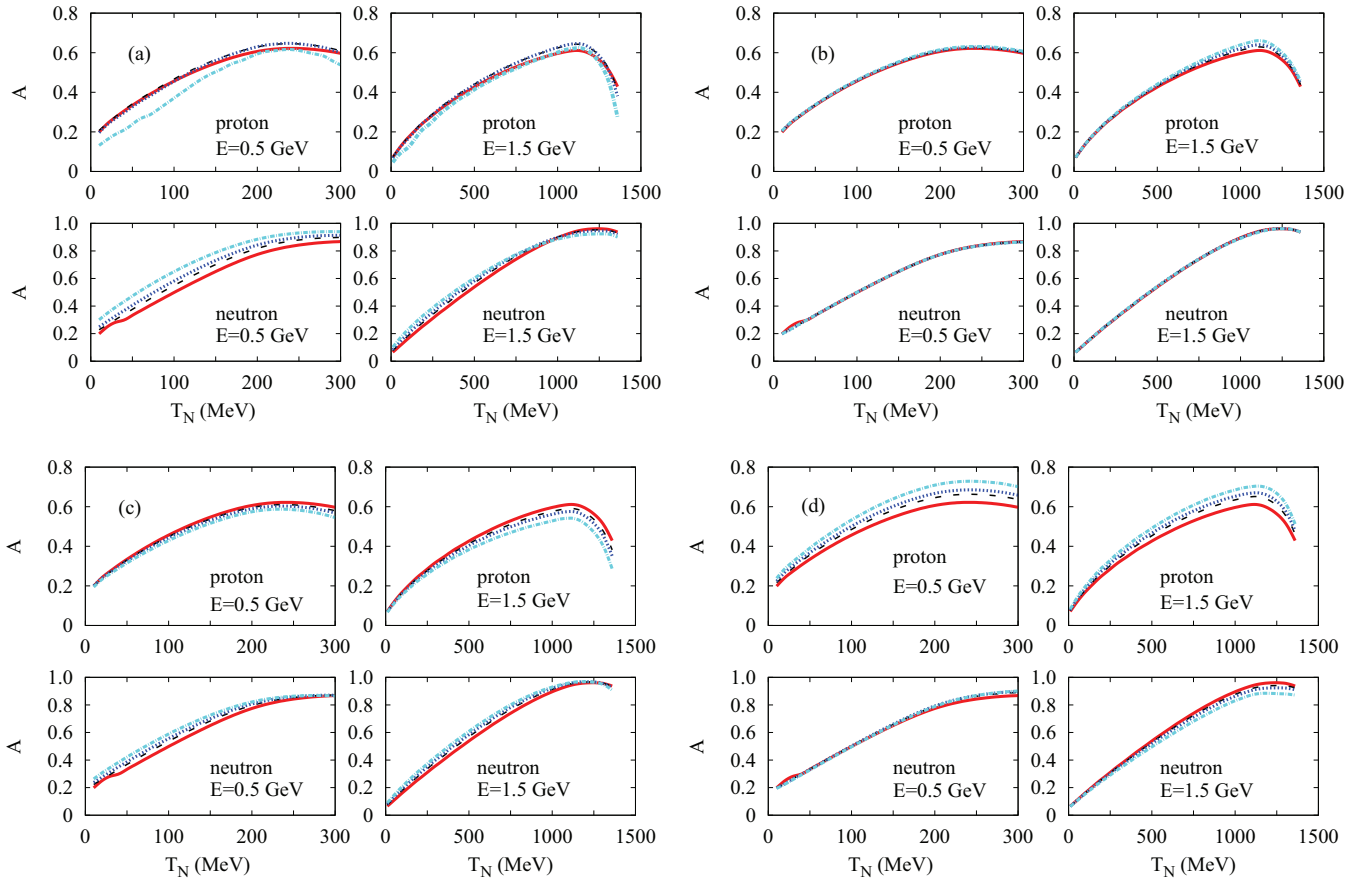

FIG. 7. (Color online) The asymmetry with the same kinematics as in Fig. 2.

sections given by

$$A = \frac{\sigma^{\nu} - \sigma^{\bar{\nu}}}{\sigma^{\nu} + \sigma^{\bar{\nu}}}, \tag{9}$$

where $\sigma^{\nu(\bar{\nu})}$ denotes the differential cross sections for the $\nu(\bar{\nu})$. Figure 7 shows the asymmetries with the same kinematics and the same explanation of the curves as Fig. 2. The effects of the density dependence on F_1 are also small similar to other cases of cross sections, but in the case of the proton with 1.5 GeV the effects increase the asymmetry within a few percent. In the case of F_2 the effects reduce the asymmetry in the proton but enhance it in the neutron. The effects on G_A increase the asymmetry except in the case of the neutron with 1.5 GeV. Therefore, in the Fig. 7(a), which is the density dependence in all form factors, the effects increase the asymmetry in the neutron but in the proton they reduce it.

Finally, in Fig. 8, we calculate the flux-averaged differential cross section $\langle d\sigma/dQ^2\rangle$ per nucleon, $\nu N \to \nu N$ and $\bar{\nu} N \to \bar{\nu} N$, and compare our results with the MiniBooNE data [8], i.e., νNCE and $\bar{\nu}$NCE. The solid (red) line is the result for the free space form factor, the dashed (black) line is for $\rho = 0.6\rho_0$, the dotted (blue) line is for $\rho = 1.0\rho_0$, and the dash-dotted (sky blue) curve is for $\rho = 2.0\rho_0$. The density dependence for $\rho = 0.6\rho_0$, $\rho = 1.0\rho_0$, and $\rho = 2.0\rho_0$ reduces the flux-averaged differential cross section about 20%, 30%, and 45%, respectively. Our result of the free space form factor is below the data about 50%. To compensate for the deviation from the data, we calculate the differential cross section for the free space form factor with the axial mass $M_A = 1.39$ GeV, which is extracted from the MiniBooNE data [8]. The dash-dot-dotted (yellow) curve is the result for $M_A = 1.39$ GeV. The result for $M_A = 1.39$ GeV enhances the differential cross section with higher Q^2. In the low-Q^2 region, the deviation from the data is about 20% but it overestimates the data in the high-Q^2 region ($Q^2 > 0.8(\mathrm{GeV}/c)^2$). Notice that we do not change the

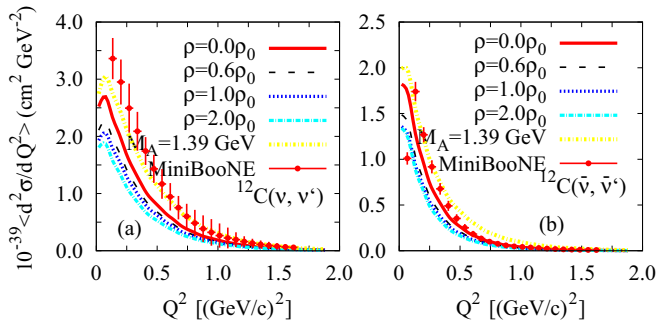

FIG. 8. (Color online) Flux-averaged differential cross sections $\langle d\sigma/dQ^2\rangle$ per nucleon, $\nu N \to \nu N$ and $\bar{\nu} N \to \bar{\nu} N$. The solid (solid) curve is the result for no density-dependence, the dashed (black) curve is for $\rho = 0.6\rho_0$, the dotted (blue) curve is for $\rho = 1.0\rho_0$, the dash-dotted (sky blue) curve is for $\rho = 2.0\rho_0$, and the dash-dot-dotted (yellow) curve is for no density-dependence. The experimental data are from the MiniBooNE experiment [8], νNCE and $\bar{\nu}$NCE.

strange quark form factor $g_A^s = -0.19$ because its contribution is small [32]. Furthermore, the target of the experimental data is CH_2 and the contribution of the hydrogen is about 14% [7,8]. However in this work only carbon is used as a target.

IV. SUMMARY AND CONCLUSION

In this work, we investigate the effects of density-dependent form factors on the differential cross sections for the inclusive (e,e') reaction and the NC reaction of $A(\nu,\nu')$ and $A(\bar{\nu},\bar{\nu}')$ scattering in the framework of a relativistic single-particle model. The density effects reduce the cross sections in both incident neutrinos and antineutrinos. We study the roles of the density dependence in each form factor (F_1, F_2, and G_A). The effects on G_A are biggest and those on F_1 are very small. We also investigate the effects on each response cross section. In the case of the proton, the effects increase the longitudinal cross sections because the contribution to F_2 is largest. Shapes of the longitudinal and transverse cross sections are the same as those of the corresponding differential cross sections but the interference term is different. The main contribution turns out to appear at the transverse cross section by comparing the magnitude. However, the effects increase the asymmetry in the proton except in the case of F_2.

Finally, we calculate the flux-averaged differential cross section in terms of four-momentum squared. The effect of density dependence reduces the cross sections and we compare this data with the experimental data. Our result with the free space form factor is below about 50%. To cure this discrepancy, we use different axial mass $M_A = 1.39$ GeV. As a result, in the low-Q^2 region, the flux-averaged differential cross section is increased about 20% but, in the high-Q^2 region ($Q^2 > 0.8$ GeV^2), the cross section is larger than the data, although this model has been successful for electron scattering.

In conclusion, our results taking into account the density dependence of the weak form factors as well as modulating the axial mass up to $M_A = 1.39$ GeV do not successfully describe the MinBooNE data. In the future, various model calculations including the improvement of our current nuclear model will be necessary to reproduce the MinBooNE data. This will shed light on the nuclear responses, especially to weak probes.

ACKNOWLEDGMENTS

This work was supported by the National Research Foundation of Korea (Grants No. 2012R1A1A2041974, No. 2014R1A2A2A05003548, and No. 2012M7A1A2055605).

[1] C. J. Horowitz *et al.*, Phys. Rev. C **85**, 032501 (2012).
[2] M. B. Tsang *et al.*, Phys. Rev. C **86**, 015803 (2012).
[3] K. S. Kim and M.-K. Cheoun, J. Phys. Soc. Jpn. **82**, 024201 (2013).
[4] O. Moreno, P. Sarriguren, E. Moya de Guerra, J. M. Udias, T. W. Donnelly, and I. Sick, Nucl. Phys. A **828**, 306 (2009).
[5] K. Patton, J. Engel, G. C. McLaughlin, and N. Schunck, Phys. Rev. C **86**, 024612 (2012).
[6] K. Abe *et al.*, Phys. Rev. Lett. **56**, 1107 (1986); L. A. Ahrens *et al.*, Phys. Rev. D **35**, 785 (1987).
[7] A. A. Aguilar-Arevalo *et al.* (MiniBooNE Collaboration), Phys. Rev. D **81**, 092005 (2010).
[8] A. A. Aguilar-Arevalo *et al.* (MiniBooNE Collaboration), Phys. Rev. D **82**, 092005 (2010).
[9] A. A. Aguilar-Arevalo *et al.* (MiniBooNE Collaboration), Phys. Rev. D **88**, 032001 (2013).
[10] A. A. Aguilar-Arevalo *et al.* (MiniBooNE Collaboration), arXiv:1309.7257.
[11] J. Nieves, I. Ruiz Simo, and M. J. Vicente Vacas, Phys. Lett. B **707**, 72 (2012); J. Nieves, F. Sánchez, I. R. Simo, and M. J. Vicente Vacas, Phys. Rev. D **85**, 113008 (2012).
[12] A. Meucci, M. B. Barbaro, J. A. Caballero, C. Giusti, and J. M. Udias, Phys. Rev. Lett. **107**, 172501 (2011); A. Meucci, C. Giusti, and F. D. Pacati, Phys. Rev. D **84**, 113003 (2011).
[13] A. V. Butkevich and D. Perevalov, Phys. Rev. C **84**, 015501 (2011).
[14] A. M. Ankowski, Phys. Rev. C **86**, 024616 (2012).
[15] J. E. Amaro, M. B. Barbaro, J. A. Caballero, T. W. Donnelly, and C. F. Williamson, Phys. Lett. B **696**, 151 (2011).
[16] R. Gonzalez-Jimenez, M. V. Ivanov, M. B. Barbaro, J. A. Caballero, and J. M. Udias, Phys. Lett. B **718**, 1471 (2013).
[17] J. Aubert *et al.*, Phys. Lett. B **123**, 275 (1983); J. Ashman *et al.*, *ibid.* **206**, 364 (1988).
[18] D. H. Lu *et al.*, Nucl. Phys. A **634**, 443 (1998); K. Saito, K. Tsushima, and A. W. Thomas, Phys. Lett. B **465**, 27 (1999).
[19] I.-T. Cheon and M. T. Jeong, J. Phys. Soc. Jpn. **61**, 2726 (1992); M. T. Jeong and I.-T. Cheon, Phys. Rev. D **43**, 3725 (1991).
[20] D. H. Lu, K. Tsushima, A. W. Thomas, A. G. Williams, and K. Saito, Phys. Lett. B **441**, 27 (1998); Phys. Rev. C **60**, 068201 (1999).
[21] D. H. Lu, A. W. Thomas, K. Tsushima, A. G. Williams, and K. Saito, Phys. Lett. B **417**, 217 (1998).
[22] K. Saito, K. Tsushima, and A. W. Thomas, Nucl. Phys. A **609**, 339 (1996); Phys. Rev. C **55**, 2637 (1997).
[23] K. Tsushima, K. Saito, J. Haidenbauer, and A. W. Thomas, Nucl. Phys. A **630**, 691 (1998); Pierre A. M. Guichon, A. W. Thomas, and K. Tsushima, *ibid.* **814**, 66 (2008); K. Tsushima and F. C. Khanna, Phys. Rev. C **67**, 015211 (2003); J. Phys. G **30**, 1765 (2004).
[24] K. Tsushima, H. Kim, and K. Saito, Phys. Rev. C **70**, 038501 (2004).
[25] M. K. Jones *et al.*, Phys. Rev. Lett. **84**, 1398 (2000).
[26] S. Malov *et al.*, Phys. Rev. C **62**, 057302 (2000).
[27] M.-K. Cheoun *et al.*, Phys. Lett. B **723**, 464 (2013).
[28] M.-K. Cheoun, K.-S. Choi, K. S. Kim, K. Saito, T. Kajino, K Tsushima, and T. Maruyama, Phys. Rev. C **87**, 065502 (2013).
[29] K. S. Kim, M.-K. Cheoun, and W. Y. So, Phys. Rev. C **90**, 017601 (2014).

[30] C. J. Horowitz and B. D. Serot, Nucl. Phys. A **368**, 503 (1981).
[31] K. S. Kim, L. E. Wright, Y. Jin, and D. W. Kosik, Phys. Rev. C **54**, 2515 (1996); K. S. Kim, L. E. Wright, and D. A. Resler, *ibid.* **64**, 044607 (2001); K. S. Kim and L. E. Wright, *ibid.* **72**, 064607 (2005); K. S. Kim, B. G. Yu, and M. K. Cheoun, *ibid.* **74**, 067601 (2006).
[32] K. S. Kim, M.-K. Cheoun, and B. G. Yu, Phys. Rev. C **77**, 054604 (2008); K. S. Kim, B. G. Yu, M. K. Cheoun, T. K. Choi, and M. T. Chung, J. Phys. G **34**, 2643 (2007).
[33] K. S. Kim and M.-K. Cheoun, Phys. Rev. C **83**, 034607 (2011).
[34] V. Bernard, L. Elouadrhiri, and U.-G. Meissner, J. Phys. G **28**, R1 (2002).
[35] D. B. Day *et al.*, Phys. Rev. Lett. **59**, 427 (1987).